

Master's thesis

Wave Dissipation and Breaking Probability

Internship directed by F.Ardhuin, Service Hydrographique et
Océanographique de la Marine, Brest

Jean-François FILIPOT

MASTER2 Physique Ocean Atmosphère, UBO, Brest

3rd year, Ecole nationale des ponts et chaussées, Champs-sur-Marne

5th October 2007

Acknowledgments

I am grateful to Fabrice Arduin for proposing me this internship and the related PhD thesis, and I thank him too, for his receptivness and for all his relevant advices. I thank Pr. Alexander Babanin for kindly providing me data, matlab scripts and help. I thank Florent Birrien, Rudy Magne and Nicolas Rascle for the assistance they provide me all along the internship.

Abstract

The aim of the present report is to study the wave dissipation due to white capping. Especially, the directional features will be investigated. Different parametrizations of the dissipation term in wave models have been proposed, yet, none is entirely satisfying. For example, the latter parametrizations could be responsible for mispredictions in oblique fetch conditions or in combined wind-sea and background swell conditions. Observations by Banner et al. (2000), show that white caps only appeared when the non-dimensional frequency spectrum, henceforth referred to as saturation, exceeds a threshold. In the present work, a saturation depending on the direction will be implemented in the wave model WAVEWATCH III. The results are compared with wave spectra observations (Hwang et al. 2000) deduced from topography acquired by an airborne scanning lidar system. In a second part, the directional dependence of the breaking probability and severity of dominant waves is investigated. To achieve this, breaking waves observations, gathered in lake George (Australia) and provided by A. Babanin are analysed. The essential wave directionality is obtained with the Wavelet Directional Method developed by Donelan et al. (1996).

Contents

I.	INTRODUCTION	2
A.	Wave Spectrum	2
1.	Wave Spectrum Definition	2
B.	The Spectral Balance	3
1.	The Wind Input : S_{in}	3
2.	The Non-Linear Interaction Source Term	5
3.	The White-capping Dissipation : S_{ds}	5
C.	Spectral parametrization of dissipation	5
1.	The Pulse Model, Hasselmann (1974), Donelan and Yuan (1994)	5
2.	The Saturation-Based Models	7
II.	DIRECTIONAL BREAKING PROBABILITIES	9
A.	Introduction	9
1.	The data	9
2.	The Wavelet Directional Method	9
3.	Results	13
III.	COMPUTATION OF A NEW DISSIPATION TERM	17
A.	Directionality and dissipation source term	17
1.	The new dissipation source term	17
2.	Bimodal properties observations	17
3.	Results	18
IV.	CONCLUSION	23
	Bibliography	25

I. INTRODUCTION

Wave breaking is the major energy sink term for waves on the sea surface, yet this phenomenon is poorly understood and thus badly estimated. Improvements in whitecapping comprehension and parametrization is then obvious for wave forecasting. Furthermore, wave-breaking is the dominant mechanism of air sea gas transfers and it also impacts strongly the remote sensing of winds, surface currents, ocean color and salinity using passive radiometry. In particular, the occurrence of whitecaps creates a very strong surface brightness temperature signal that dominates by far the salinity signal (e.g. Reul and Chapron 2003). Surface salinity measurements with the soon-to-be launched SMOS mission will be impossible without flagging of possibly correcting for white capping effects. Estimation of wave breaking scales and intensity from a numerical wave model could thus benefit to a wide array of applications. A great number of theories have been proposed to represent the white capping, however none is entirely reliable. The aim of the present report is then to investigate ways of improving wave breaking parametrization. Especially the relationship between wave breaking and wave directions will be studied. Firstly, we analyse wave breaking observations to determine if there is a variation in wave breaking probability with different wind and waves directions. Based on this analysis we investigate the effect of a direction dependant dissipation source term in the numerical model WAVEWATCH III.

A. Wave Spectrum

1. Wave Spectrum Definition

The Navier Stokes equations for an inviscid and irrotational fluid over a flat bottom at depth D , lead to Bernoulli's and mass conservation equation:

$$\frac{\partial \phi}{\partial t} = -\frac{1}{2} \left[|\nabla \phi|^2 + \left(\frac{\partial \phi}{\partial z} \right)^2 \right] - \frac{p}{\rho_w} - g\eta + C(t), \quad (1.1)$$

$$\nabla \cdot \mathbf{u} + \frac{\partial w}{\partial z} = \nabla^2 \phi + \frac{\partial^2 \phi}{\partial z^2} = 0, \quad -D \leq z \leq \eta, \quad (1.2)$$

Where ϕ is the velocity potential, η , the sea surface elevation, p the pressure, ρ_w the fluid density and g the gravity.

Under small perturbations assumptions, Airy (1845) demonstrates that 1.1 is given by:

$$\frac{\partial \phi}{\partial t} = -g\eta - \frac{P_a}{\rho}, \quad (1.3)$$

Moreover, the sea surface is considered to be solid:

$$w = \frac{d\eta(x, y, t)}{dt} \quad \text{at} \quad z = 0, \quad (1.4)$$

Assuming $|\nabla \eta|$ and $\eta/D \ll 1$, the surface kinematic boundary condition simplifies as:

$$\frac{\partial \phi}{\partial z} = \frac{\partial \eta(x, y, t)}{\partial t} \quad \text{at} \quad z = \eta, \quad (1.5)$$

Airy (1845) found a solution of this set of equation, using the variable separation method. In deep water $\zeta = ae^{i(\mathbf{k} \cdot \mathbf{x} - \sigma t)}$ is a solution therefore, by the vertue of linearity every superposition of solutions is still a solution of the approximate linear equation. The sea surface can thus be represented by a fourier decomposition:

$$\eta(x, y, t) = \sum_{i=1}^N a_i e^{i(\mathbf{k}_i \cdot \mathbf{x} - \sigma_i t)}, \quad (1.6)$$

Where a_i , \mathbf{k}_i and σ_i are respectively the amplitude, wave vector and frequency associated with the wave component i and are related by the Laplace's (1776) dispersion relation:

$$\sigma^2 = gk \tanh(kD), \quad (1.7)$$

The energy density of a linear wave train per unit surface is (e.g. Lamb 1932) :

$$E = \frac{1}{8} \rho_w g H^2, \quad (1.8)$$

Therefore, the average energy by mass unity of the previous wave field is:

$$\frac{\overline{E}}{\rho_w g} = \frac{1}{8N} \sum_{i=1}^N H_i^2 = \frac{1}{2N} \sum_{i=1}^N a_i^2 = \sigma^2, \quad (1.9)$$

Where σ^2 is the variance of the signal. The amplitudes a_i are thus related to the energy and are frequency and direction dependent. The a_i frequency-direction distribution is the discrete amplitude spectrum which becomes the continuous spectrum $F(f, \theta)$ in the limit as $N \Rightarrow \infty$, where:

$$F(f, \theta) \Delta f \Delta \theta = \frac{a_i^2}{2}, \quad (1.10)$$

The variance σ^2 may thus be expressed by:

$$\sigma^2 = \int_0^{2\pi} \int_0^\infty F(f, \theta) \Delta f \Delta \theta, \quad (1.11)$$

$F(f, \theta)$ is finally the directional frequency spectrum.

B. The Spectral Balance

The temporal and spatial evolution of the spectrum is driven by three major forcings : the wind input, the wave-wave interactions and the dissipation due to whitecapping, bottom friction or interaction with turbulence :

$$\frac{DE}{Dt} = S_{in} + S_{nl} + S_{ds}, \quad (1.12)$$

1. The Wind Input : S_{in}

Waves are created by fluctuations in the normal pressure exerted by the wind on the sea surface, which is why they are nearly irrotational. Jeffreys (1924,1925) showed that these variations lead to an energy flux from the atmosphere to the ocean :

$$\frac{\partial E}{\partial t} = \frac{1}{\rho_w} p \frac{\partial \eta}{\partial t}, \quad (1.13)$$

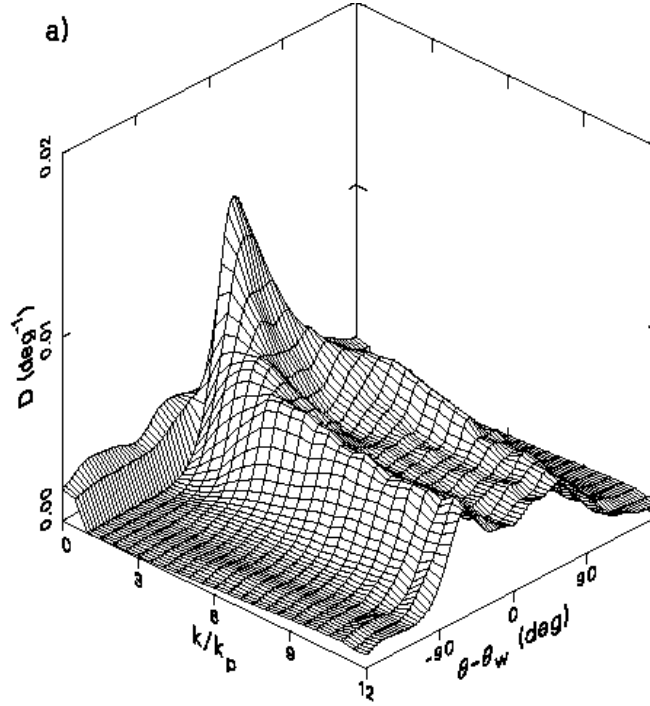


Figure 1.1: Measured spectrum, Long et Resio, 2007.

$$\frac{\partial \phi}{\partial t} = \frac{p}{\rho_w} - g\zeta - \frac{P_a}{\rho_w} \quad \text{at } z = 0 \quad (1.14)$$

Combining 1.3 and 1.5, yields:

$$\frac{\partial^2 \phi}{\partial t^2} + g \frac{\partial \phi}{\partial z} = \frac{1}{\rho} \frac{\partial P_a}{\partial t} \quad \text{at } z = 0 \quad (1.15)$$

The response to the atmospheric pressure can be interpreted as a resonance phenomenon. A wave train can be regarded as an oscillator with its wavenumber k and frequency $\sigma = kc$ where c is the phase speed. For simplification, let us consider the effect of the atmospheric turbulence as a single sinusoidal perturbation : $P_a = B \cos(\mathbf{k}_a \cdot (\mathbf{x}_U t))$. Any pressure field can be recovered by superposition of such perturbation. Hence, the sea surface is forced with a wave number k_a at the frequency $k_a U$. Resonance appears when the wind speed reaches the phase velocity of an Airy wave which wave number is k_a . Philipps (1957) proposed that air pressure fluctuations due to turbulence could explain wind-wave generation. This theory explains the initial wave growth, yet the assumption of an homogenous wave field is not valid as soon as the waves disturb the wind. Miles (1957) developed a theory which took account of that latter issue : The presence of waves induces changes in the atmospheric forcing. This modification, linearized, is given by :

$$P_a = (\alpha_r + i\alpha_i) \rho_a g a e^{i(\mathbf{k} \cdot \mathbf{x} - \sigma t)} \quad (1.16)$$

Introducing the pressure fluctuation in 1.1 yields

$$\frac{\partial E(f, \theta)}{\partial t} = -\beta \sigma E(f, \theta), \quad (1.17)$$

Where $\beta = \alpha_i \rho_a / \rho_w$ is a non-dimensional growth rate that can be calculated by solving the Orr-Sommerfeld equation for the air flow (Miles, 1957, Haistov, 2003) . Hence the part of the pressure variation that contribute to the wave growth or decrease is in phase with the slope. The wind input source term can thus be expressed by: $S_{in} = -\beta \sigma E(f, \theta)$, for which many parametrizations have been proposed. Miles (1957) proposed for example:

$$S_{in} = \epsilon \gamma \omega \left(\frac{u_*}{c} \right)^{1/2} \cos^2 \theta \quad (1.18)$$

Where ϵ is the air-sea density ratio, u_* the friction velocity, ω and c the wave frequency and velocity, θ the angle between the wind and the wave propagation direction and γ is the Miles' parameter.

2. The Non-Linear Interaction Source Term

At the first order in slope, the equations are linear and each spectral component behaves independently, however at higher order interactions among waves occur. This interaction results in energy transfers between the components (Philips, 1960). In shallow water ($kD \ll 1$) energy exchanges appear at second order resulting in an energy exchange among three wave trains. but in deep water resonance only occurs at third order corresponding to an exchange of energy among four wave trains with wavenumber $\mathbf{k}_1, \mathbf{k}_2, \mathbf{k}_3, \mathbf{k}_4$ (Hasselmann 1961, 1962). Hasselmann (1962) gives the non-linear source term in the form :

$$\begin{aligned} \frac{\partial E(\mathbf{k})}{\partial t} &= S_{nl}(\mathbf{k}) \\ &= \int |T(\mathbf{k}_1, \mathbf{k}_2, \mathbf{k}_3, \mathbf{k})|^2 \delta(\mathbf{k}_1 + \mathbf{k}_2 - \mathbf{k}_3 - \mathbf{k}_4) \delta(\sigma_1 + \sigma_2 - \sigma_3 - \sigma_4) \\ &\quad \times [E(\mathbf{k}_1) E(\mathbf{k}_2) (E(\mathbf{k}_3) + E(\mathbf{k}_4)) - E(\mathbf{k}_3) E(\mathbf{k}_4) (E(\mathbf{k}_1) + E(\mathbf{k}_2))] d\mathbf{k}_1 d\mathbf{k}_2 d\mathbf{k}_3, \end{aligned} \quad (1.19)$$

Interactions among four waves are responsible for an energy cascade toward both high and low frequencies. This phenomenon partly explains that the wave period increases with the fetch and that fully developed waves propagate faster than the wind. S_{nl} conserves the total energy $\int E(\mathbf{k}) d\mathbf{k}$, as well as the momentum $\int \mathbf{k} E(\mathbf{k}) / \sigma d\mathbf{k}$ and the wave action $\int \mathbf{k} E(\mathbf{k}) / \sigma d\mathbf{k}$. Unfortunately the exact calculation is far too expensive for operational wave forecasting, most the models used then a Direct Approximation Interaction (DIA, Hasselmann et al 1985). This approximation used the conservation properties of the energy, action and momentum of the resonant quadruplets, $\mathbf{k}_1, \mathbf{k}_2, \mathbf{k}_3, \mathbf{k}_4$. However the DIA holds only one geometrical configuration for each spectral component. Although the DIA conserves the waves properties, the shape of the related S_{nl} is different from the theoretical shape. Especially, this approximation is responsible for a too wide directional distribution of S_{nl} .

3. The White-capping Dissipation : S_{ds}

Wind provides energy to the wave field, as a result, the amplitude of the waves increases. This process continues until the waves become unstable and break. For periodic, symmetrical waves, breaking occurs when the velocity of the crest u_c reaches the phase speed c . This condition is found to correspond to the $H/L \simeq 0.14 \tanh(kD)$ (Miche (1944)). However for irregular waves there is no such simple simplification. Wave breaking is then strongly related to wave slope. Mason (1951) splits the white caps in two different categories: the plunging breakers and the spilling waves. In the first case, the wave crest hits violently the forward face of the wave. In the second case, the white cap is due to a free surface instability near the wave crest. This two phenomenon lead to the same results: a flow separation. The separation occurs at a slope discontinuity, where the flow upstream is smooth and the flow downstream is turbulent and thus irrotational (Longuet-Higgins, 1973). In the turbulent area, water and air are mixed and consequently, the local density is less than the density in the laminar zone.

Many theories have been advanced to explain and quantify this dissipation, let us introduce some of them.

C. Spectral parametrization of dissipation

1. The Pulse Model, Hasselmann (1974), Donelan and Yuan (1994)

This theory assumes that white caps are a random distribution of pressure pulse on the sea surface and are geometrically similar. White caps are preferentially located on the forward face of the

waves, therefore they generally remove energy to the wave field. If the white-cap exerted a pressure P_w on a sinusoidal wave $\eta = \sin\omega t$, it follows that $p_w \sim \rho_w g h_w \sim \rho_a g a$. Consequently the energy flux can be written :

$$\frac{\partial E}{\partial t} = \frac{1}{\rho_w} \overline{p_w \frac{\partial \zeta}{\partial t}} \quad (1.20)$$

Thus,

$$S_{ds}(k, \theta) = -\gamma_{ds} \omega E(k, \theta) \quad (1.21)$$

Where γ_{ds} is a attenuation coefficient related to non-local properties. Other aspects of the dissipation have also been highlighted by Banner et al. (1989). They show that high frequency waves are attenuated in the wake of large breakers. Furthermore, the steepness of waves seems to be a relevant parameter to mesure the magnitude of the dissipation. Gathering these kind of informations, Komen et al (1984) proposed a form for S_{ds} such that :

$$S_{ds}^{KHH}(k, \theta) = -C_{ds} \left(\frac{\hat{\alpha}}{\hat{\alpha}_{PM}} \right)^m \left(\frac{\omega}{\bar{\omega}} \right)^n E(k, \theta) \quad (1.22)$$

Where $\bar{\omega}$ is a mean frequency:

$$\bar{\omega} = \frac{\int \omega^{-1} E(\mathbf{k}) dk}{\int E(\mathbf{k}) dk}, \quad (1.23)$$

$\hat{\alpha} = \sigma^2 \bar{\omega}^4 / g^2$ is an integral steepness parameter and $\hat{\alpha}_{PM}$ is the theoretical value of $\hat{\alpha}$ for the Pierson- Moskowitz spectrum. σ^2 stands for the total energy $\sigma^2 = \int E(k, \theta) dk d\theta$. This parametrization of S_{ds} is used in some operational forecasting models such as SWAN (Booij et al. 1999). This form was adapted by Jansen (1994) to balance the S_{in} term of Janssen, it is usually referred to as "WAM cycle 4":

$$S_{ds}^{JKHH}(k, \theta) = -C_{ds} \hat{\alpha}^2 \left[\left(\frac{k}{\bar{k}} \right) \delta + \left(\frac{k}{\bar{k}} \right)^2 (\delta - 1) \right] E(k, \theta) \quad (1.24)$$

One of the main problem with this parametrization is the prediction in presence of both swell and wind-sea. In particular $\bar{\omega}$ is more weighted to the low frequencies, giving a very strong reduction in dissipation in the presence of swell, which is unrealistic (e.g. Ardhuin et al. 2007). Another problem is the absence of specific dissipation or attenuation mechanism for swells, which implies large biases in models results:

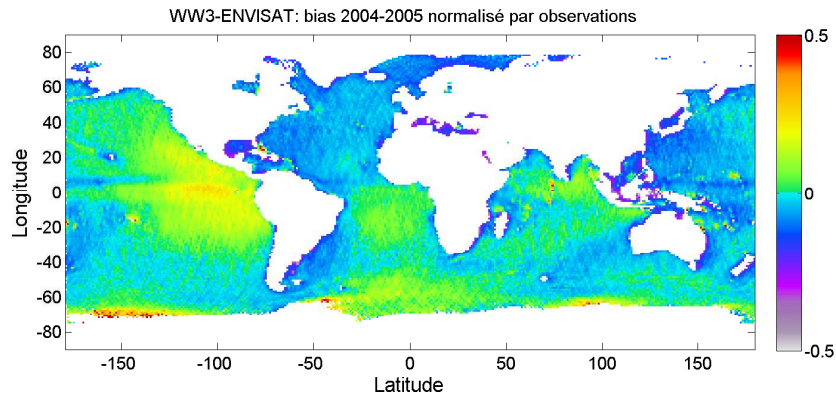


Figure 1.2: H_s normalized bias between ENVISAT measurements and WAVEWATCH predictions.

Usually, a background swell does not change the wind-sea growth. Yet, in presence of swell the mean frequency $\bar{\omega}$ is then lower than if there were only wind-sea. Therefore (Donelan (1987)), the dissipation source terms causes too much energy loss at high frequency, and opositely, the lower frequencies are not enough attenuated. Holthuijsen et Booij (2000) proposed to remove the spurious dependance of the wind-sea growth in the swell by making S_{ds} only dependant on higher frequencies than the frequency considered. Yet, swell was still too much dissipated. The Cumulative Steepness Method proposed by Hurdle and Van Veddler (2004) lies on the straining principle which assume that short waves are steepen (and then may break) when they are riding on longer waves. The dissipation at a given frequency f_i is here a function of the sum of the steepness of all spectral components above f_i . If the wind sea is successfully decoupled from the swell according to this theory, the model encounter troubles to reproduce the statistics of pure wind-sea. Bidlot et al. (2005), reverted to the original definition of the mean spectral wave number by komen et al. (1984) giving more weight to the higher frequencies.

$$\bar{k}_{BAJ} = \frac{\int \sqrt{k} E(k) dk}{\int E(k) dk} \quad (1.25)$$

Ardhuin et al. (2007) demonstrate that this approach attenuates but does not remove the artificial swell effect.

2. The Saturation-Based Models

Based on observations of waves breaking in varying currents, Phillips (1974) suggested that S_{ds} was a non linear function of the spectrum, strongly increasing with increasing energy. Such a dependence is best expressed by putting the wave spectrum in non dimensional form:

$$B(k_x, k_y) = k^4 E(k_x, k_y) \quad (1.26)$$

Observation by Banner et al. (2000) have further shown that whitecaps appeared only when the frequency-directionally integrated spectrum exceeds a threshold. Based on this assumptions, Alves and Banner (2000) modified the WAM cycle 3 dissipation term (WAMDI 1988) and proposed a S_{ds} parametrization based on this threshold behaviour:

$$S_{ds}(k, \theta) = -C_{ds} \left(\frac{B(k)}{B_r} \right)^m \left(\frac{\omega}{\bar{\omega}} \right)^{p/2} (E_{tot} k_p^2)^n E(k, \theta) \quad (1.27)$$

Where $B(k)$ is the non-dimensional spectrum integrated over directions, also referred to as saturation and easily related to the mean squared slope $mss = \int k^3 E(k, \theta) d(\ln k)$.

$$B(k) = \int B(k_x, k_y) k d\theta = k^3 \int E(k, \theta) d\theta \quad (1.28)$$

$E_{tot} k_p^2$ is an integral steepness parameter and k_p the peak frequency. m and n are constants that need to be determine to fit the observations. This form of S_{ds} shows that there is an energy loss at the scale k if the saturation $B(k)$ exceeds the limit B_r . Yet, dissipation is non zero even if there is no white capping : wave-wave and wave-turbulence interactions cause dissipation too. The exponent p is designed to represent these latter effects by keeping S_{ds} non zero even if he threshold B_r is crossed :

$$p = \frac{p_0}{2} + \frac{p_0}{2} \tanh \left\langle 10 \left(\left(\frac{B(k)}{B_r} \right)^{1/2} - 1 \right) \right\rangle \quad (1.29)$$

Banner et al. 2000, proposed a breaking threshold ϵ of great interest supported by observations of breaking probabilities:

$$\epsilon = \frac{H_p k_p}{2} \quad (1.30)$$

where,

$$H_p = 4 \left(\int_{0.7f_p}^{1.3f_p} E(f) df \right)^{1/2} \quad (1.31)$$

ϵ measure the significant spectral peak steepness. Banner et al (2000) show high correlations between ϵ and the breaking probability in wind-sea conditions. Actually, they observed a clear breaking threshold for $\epsilon \simeq 0.55$, below which the breaking probability is zero.

In this report other forms of saturation will be investigated. Especially, the importance of the directionality will be studied. Indeed, in the case of saturation based dissipation, the major variable, namely the saturation $B(k)$ is integrated over the directions. In the present report we will try to investigate a saturation depending on the direction θ . This approach will be more detailed in the related part. Wave breaking observations could also enable significant improvement concerning the parametrization of the dissipation. Waves observations could provide breaking strength and probability related to waves scales and directions. With appropriate parametrizations, these informations could be related to the spectral dissipation. A new dissipation sink term would then be the product of a breaking probability with a breaking severity, validating by observations. Such a parametrization would also be easier to generalize the surf zone where this approach have been shown to be successful for a long time (e.g. Thornton and Guza, 1983).

II. DIRECTIONAL BREAKING PROBABILITIES

A. Introduction

As we have seen previously, another relevant mean to describe the dissipation sink term could be to assign a breaking probability and severity to each wave scale and direction (Banner et Morrison, 2005). The loss of energy for would then the product of the related probability and severity. The first step to develop a the new dissipation source terme S_{ds} is obvioulsy to determine these probabilities and strength. Banner and Morison invetigate the breaking wave crest length spectral density $\Lambda(c)$ where c is the phase velocity. The link between $\Lambda(c)$ and S_{ds} is given by Philips (1985), based on the laboratory data of Duncan (1991).

$$S_{ds}(c)dc = bg^{-1}c^5\Lambda(c)dc \quad (2.1)$$

b is a constant which reflects the breaking strength. The authors used a saturation based dissipation source term, first proposed by Alves and Banner (2003) to produce computed $\Lambda(c)$. Lastly this $\Lambda(c)$ is compared to measurements of breaking waves crest length spectral density for several sea ages, gathered in the FAIRS experiment. This study provided breaking probabilities dependent on the phase velocity c which is related to the wavenumber. The present work will deal with the directional breaking probability of dominant breakers. By definition, the frequency f of dominant waves is ranged from $0.7f_p$ to $1.3f_p$. We actually focus our attention on dominants waves because they are responsible for the larger loss of energy in the spectrum.

1. The data

The data used in this study were kindly provided by A. Babanin. They were gathered by the mean of an experimental device installed in lake George near Canberra in southern Australia in 1997. This lake is 25 km long and 10 km wide, and is extremely shallow, indeed, the mean depth is 1m and the maximal depth is 2m. Waves observed in that location are therefore in finite depth. The observations were gathered 50m away from the shore in 1m depth. The device consists of an array of capacitance gauges, each coupled with an hydrophone. The capacitance gauges measure the surface elevation while the hydrophones detect the breaking events. The breaking detection is completmented with a video record which allows to confirm the hydrophone data. The sample frequency is respectively, 25 Hz for the surface elevation and 4 Hz for the hydrophone records. The aim of the present study is to produce directional breaking probabilities. It was thus necessary to assign a direction to each wave. To achieve this goal, we use the Wavelet Directional method developed by Donelan et al. (1996), based on the standard wavelet method implemented by Bertrand Chapron. The following table sum up wave records used, f_p is the peak frequency, H_s the wave significant height, U_{10} the wind at 10m-height, and U_{10}/c_p the wave age.

Record	f_p , Hz	H_s , m	U_{10} , m/s	age= U_{10}/c_p
(a)	0.36	0.45	19.8	0.11
(b)	0.33	0.40	15.0	0.13
(c)	0.35	0.37	12.9	0.17
(d)	0.38	0.45	12.8	0.19

2. The Wavelet Directional Method

If the Fourier Analysis provides a reliable frequency decomposition of a given signal, the temporal resolution could be insufficient. The Wavelet Directional Method provides a time frequency representation of a time or spatial serie. Yet, according to Shannon's incertitude theorem, a gain in the time resolution imply a loss in the frequency resolution. For this work we use the WDM code prior developed by Donelan et al. (1996) and the Riding Wave Removal (RWR) developped by Erick Shultz. The RWR method allows to remove short waves riding on larger waves, and makes the zero crossing

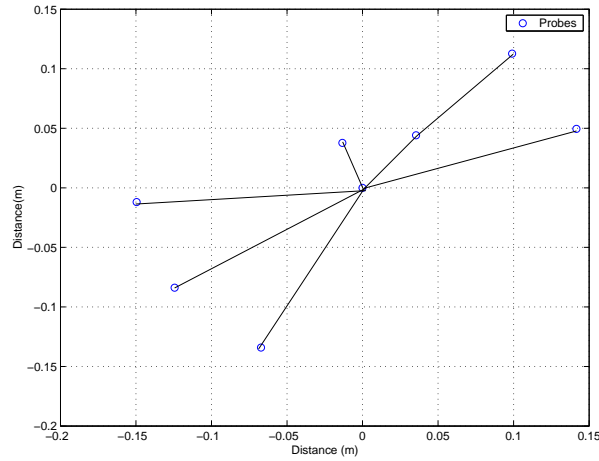


Figure 2.1: Geometry of the eight probes array

detection of dominant waves more reliable. More precisely, this algorithm removes every waves whose frequency f is greater than $1.9f_p$.

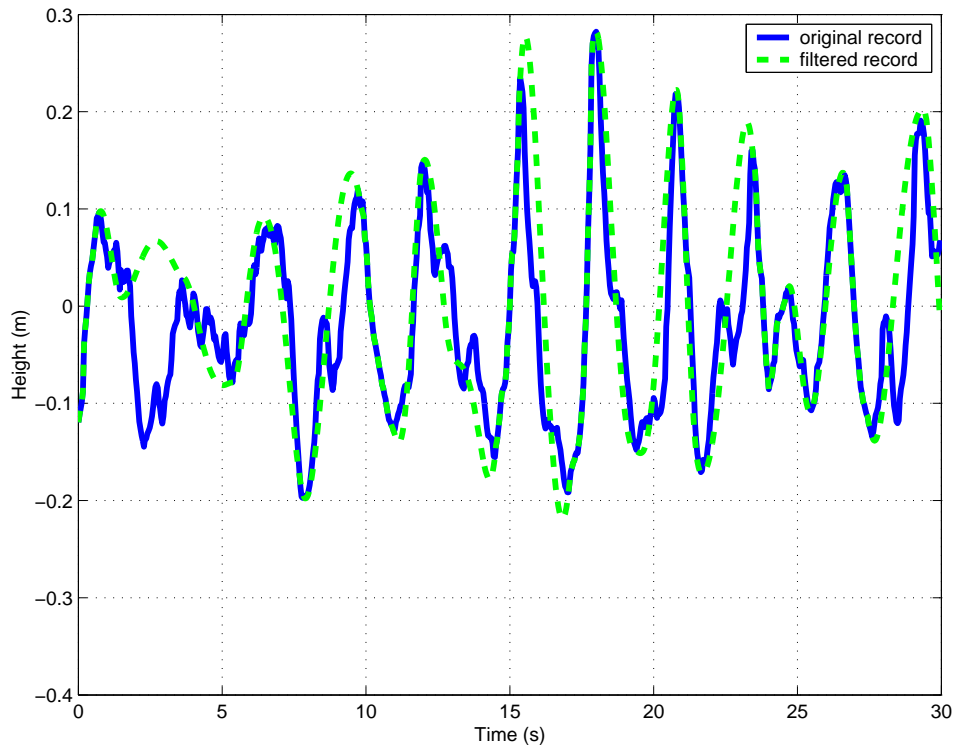


Figure 2.2: A 30s wave height record before and after the RWR implementation.

We need first to define the type of wavelets that will be used. Donelan et al. (1996) choose a wavelet family derived from the Morlet's wavelet :

$$m(t) = \frac{1}{\sigma\sqrt{\pi}} e^{it - \frac{t^2}{2\sigma^2}} \quad (2.2)$$

The frame of wavelets is then composed of translated and dilated wavelets :

$$w_{ij}(t) = \omega_j^{-1/2} m(\omega_j(t - t_i)). \quad (2.3)$$

The wavelet coefficients are thus :

$$W_{ij} = \int X(t) \overline{w_{ij}(t)} dt. \quad (2.4)$$

Therefore the time-frequency spectrum is :

$$S(t_i, \omega_j) = |W_{ij}|^2. \quad (2.5)$$

The wavelets considered here are assumed to behave like plane waves :

$$w_{ij}(t, \mathbf{k}_{ij} \cdot \mathbf{x}) = \omega_j^{-1/2} m(\mathbf{k}_{ij} \cdot \mathbf{x} - \omega_j(t - t_i)) \quad (2.6)$$

Hence, while $|\mathbf{k}_{ij} \cdot \mathbf{x}| \ll \sigma$, wavelet coefficients at a given location \mathbf{x} are related to wavelet coefficients at an arbitrary origin $x = 0$ by :

$$S(t_i, \omega_j) = |W_{ij}|^2. \quad (2.7)$$

$$W_{ij}^{\mathbf{x}} = e^{-i\mathbf{k}_{ij} \cdot \mathbf{x}} W_{ij}^0. \quad (2.8)$$

The phase shifts $\phi_{ij} = kr_{ij} \cos(\theta - \alpha)$ (where $\mathbf{r} = (r, \alpha)$ are the separation vector of pairs of staffs) between staffs recording, are easily measurable and provide the wavenumber \mathbf{k}_{ij} . Indeed, the wavenumber vectors (k, θ) may be evaluated from two pairs of staffs ab and cd :

$$k = \left[\frac{\phi_{ab}}{r_{ab} \sin \alpha_{cd}} - \frac{\phi_{cd}}{r_{cd} \sin \alpha_{ab}} \right] / [\sin(\alpha_{cd} - \alpha_{ab}) \cos \theta], \quad (2.9)$$

$$\theta = \arctan [(\Gamma \cos \alpha_{cd} - \cos \alpha_{ab}) / (\sin \alpha_{ab} - \Gamma \sin \alpha_{cd})] \quad (2.10)$$

If there are more than three wave staffs, the mean of the multiple estimations of \mathbf{k} is calculated. This analysis has the disadvantage of biasing the directional distribution, however for our application it is quite appropriate.

Moreover, in addition to the breaking probability study we investigate the severity issues, following the method described by Manasseh et al (2006). Manasseh et al (2006) propose a survey of the frequency distribution of breaking waves probability and severity based on the same data set. Supported by experiments, the severity is assumed to be related to the radii of bubbles generated by white-capping. Rayleigh (1917) suggested that individual bubbles oscillate volumetrically with a natural frequency related to their radii. A solution of the Rayleigh Plesset equation shows that this latter frequency is inversely proportional to the bubbles radii (Minnaert 1933):

$$\omega_0 = 4 \frac{1}{R_0} \sqrt{\frac{3\gamma P_0}{\rho}} \quad (2.11)$$

Where ω_0 is the radian frequency, γ is the ratio of specific heats of the gases, P_0 the absolute liquid pressure, ρ the liquid density, and R_0 is the equivalent spherical radius of the bubble.

The bubbles emit sounds that may be detected when they leave their parent body of gas. These sounds can obviously be related to ω_0 and thus to R_0 . In Manasseh et al (2006), a relevant sound pressure threshold is determined so as to discriminate wave breaking and non wave breaking events. If the threshold is exceeded, a brief pulse of sound is captured and is assumed to be due to a single freshly formed bubble. The frequency is then measured and turned into a bubble radii. As shown by figure 2.4, laboratory experiments clearly support that bubble size increase with breaking severity. The experiments consisted in measuring the wave height before and after white capping, in the mean time bubbles size was detected. Yet, it is very important to keep in mind that the exact relationship between breaking severity and bubble size is still not well established. Therefore the informations provided by the bubbles radii will be considered exclusively qualitative. In the following study, the directional distribution of the breaking severity represented by the bubbles radii will be investigated.

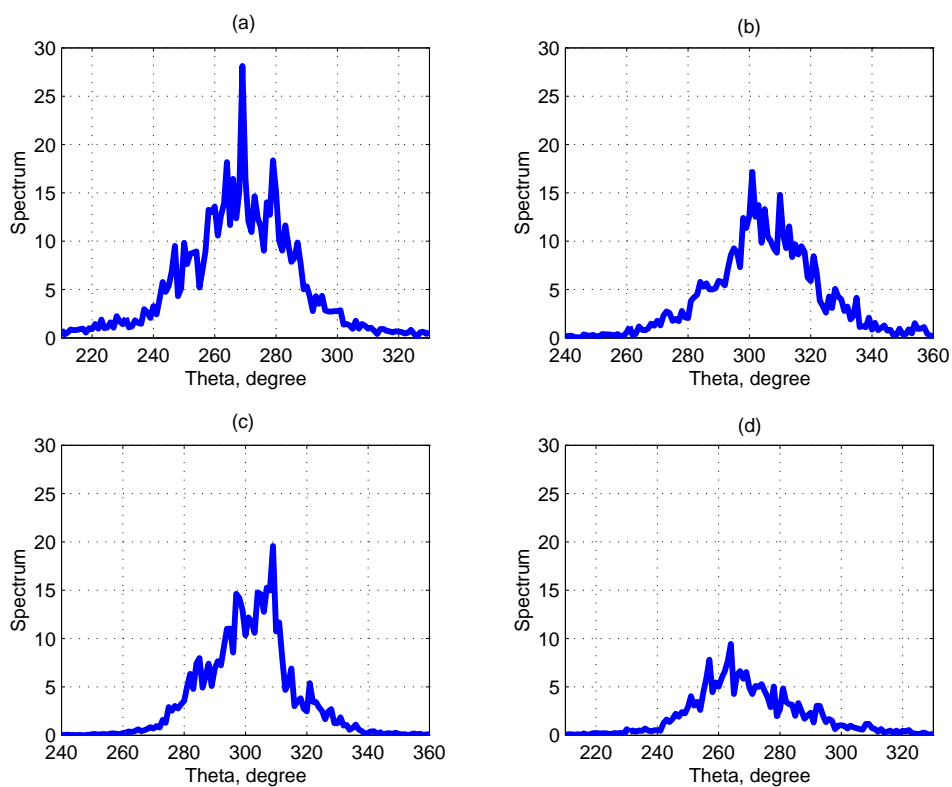


Figure 2.3: Wave spectra calculated with the WDM for records (a), (b), (c) and (d).

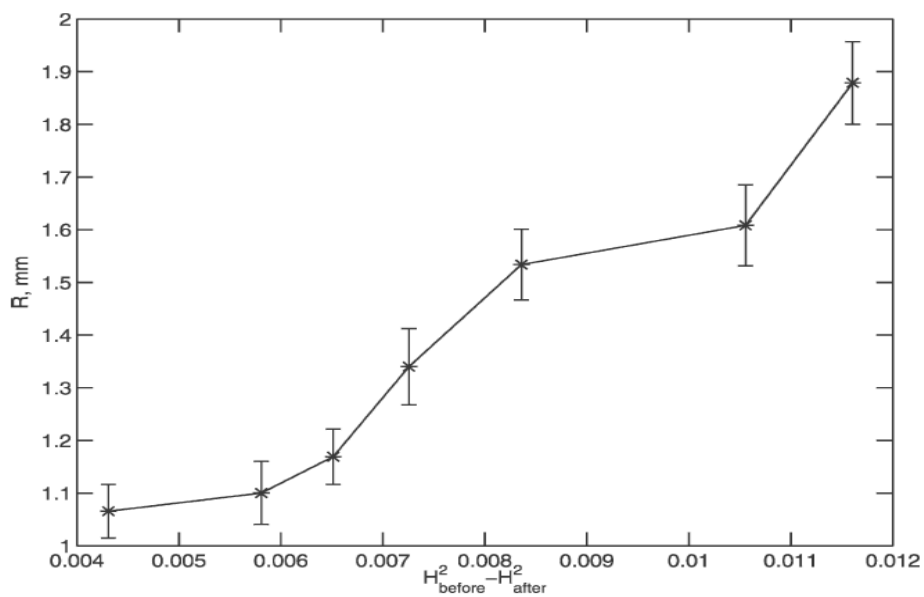


Figure 2.4: Breaking severity assumed as bubble radius R against wave energy loss. Vertical bars are for the 95% confidence limits on R . (From Manasseh et al 2006).

3. Results

For this study we have at one's disposal four time elevation series and their corresponding breaking records. The analysis process consists first in applying the WDM to the wave time series. As shown before, the wavenumber vectors were available at each time step. The next thing to do is to select the dominant waves and to detect whether they break or not. Finally, the breaking and non-breaking waves are classified by directional bins around the peak direction θ_p . There are ten directional bins, each 10° . The directional breaking probability density is thus the number of breaking waves divided by the total number of waves by direction bin. Moreover the directional width around the spectral peak or the number of bin has to be sufficiently small so that the number of waves per bin remains significant. The severity assigned for each wave is the mean bubble radius calculated over the wave time steps. If at given time step no breaking event is detected, the bubble radius is assumed to be zero. This method, enables to take into account both the number and the strength of the whitecaps riding on a given wave. The following figures present the number of wave in each directional bin N , the breaking probability $P(\theta)$, the assumed breaking strength $R(\theta)$ and finally the product $P(\theta)R(\theta)$. This latter product could be further linked to a dissipation rate related to a given direction. Each plot has been shifted in order to line the spectral peak with the direction 0° . Concerning the breaking probability, these figures do not exhibit any particular directional dependency. In the other hand, the breaking severity seems to be stronger in the peak direction. This leads the product $P(\theta)R(\theta)$ to exhibit the same kind of shape for record (a), yet such a peak is not observed for the other record. Concerning the stochastic shape of breaking severity and probability, especially the small number of waves in the direction bin located far from the peak direction could probably be accused. The shift between the peak direction and the severity maximum could be explained by the asymmetry of the spectra. In addition, the conditions observed in lake George are very specific (high wind forcing, shallow water), other observations are obviously required to conclude definitely. Besides, the Wavelet Directional Method only provide one direction for a given scale at a given time step. This is likely to cause mistake in the directional analysis. The severity used in the present study could obviously be discussed and needs further investigations. As discussed previously, the small number of waves in direction bin far from the peak direction is obviously also a likely cause of mistakes. Finally, the breaking detection could also cause some troubles, actually strong breaking events may be detected before the detection of the related wave, breaking event could then be associated to the wrong wave.

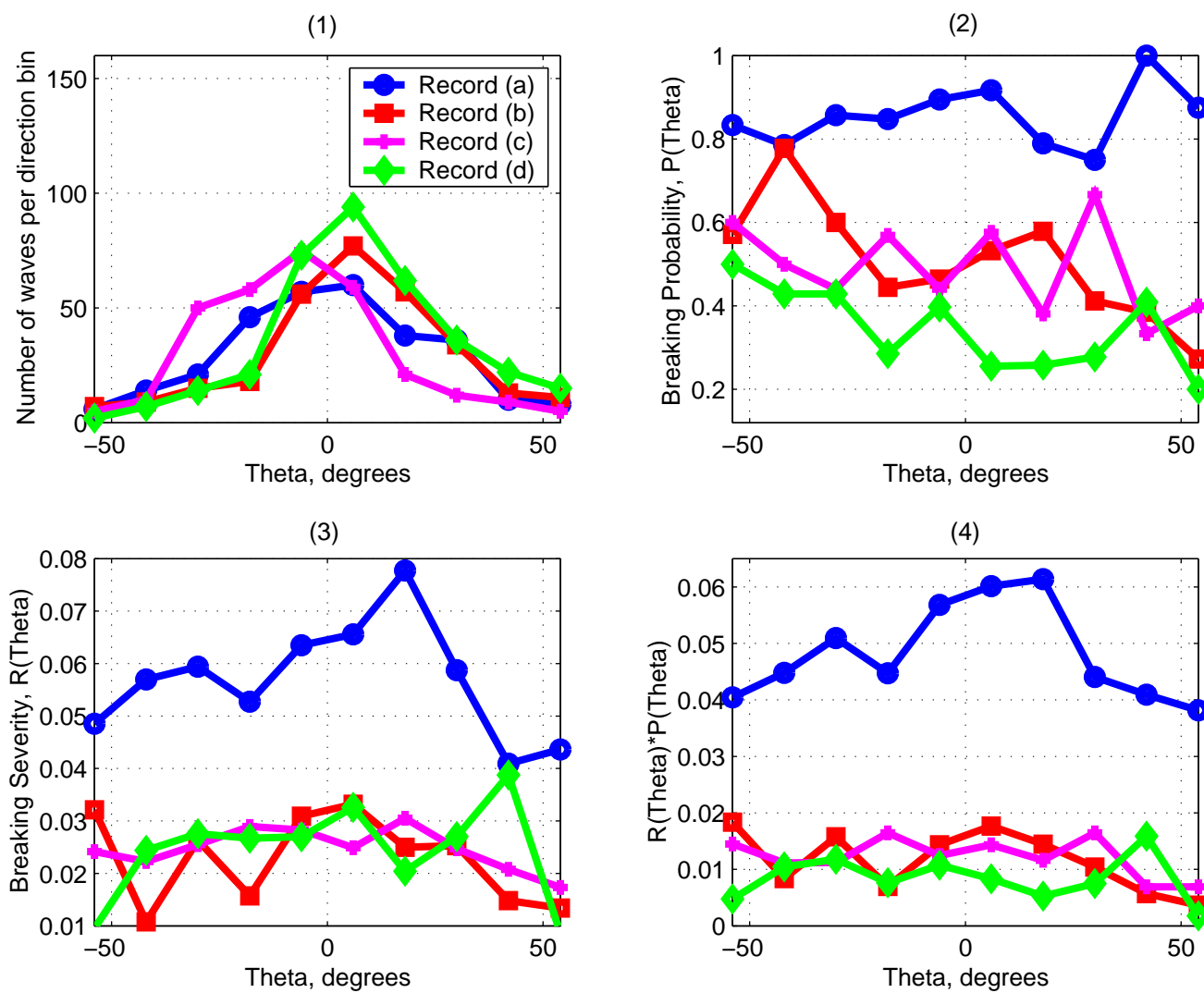


Figure 2.5: Breaking statistics: (1) number of waves per frequency bins, (2) Breaking probability $P(\theta)$ (3) Assumed breaking severity $R(\theta)$, (4) $P(\theta)R(\theta)$. For each statistic, the four records are represented .

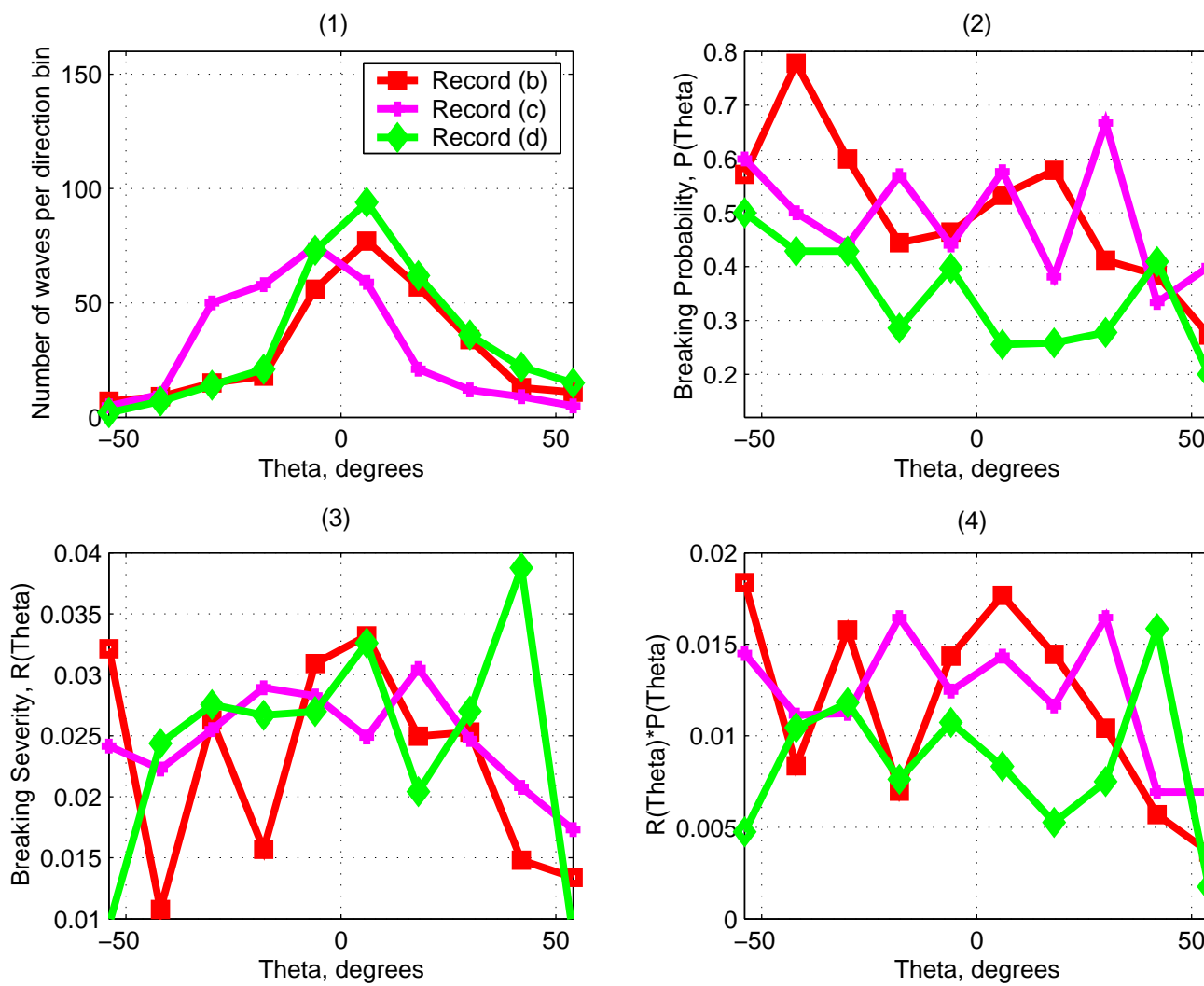


Figure 2.6: Same as the previous figure with only the three records (b), (c), (d) .

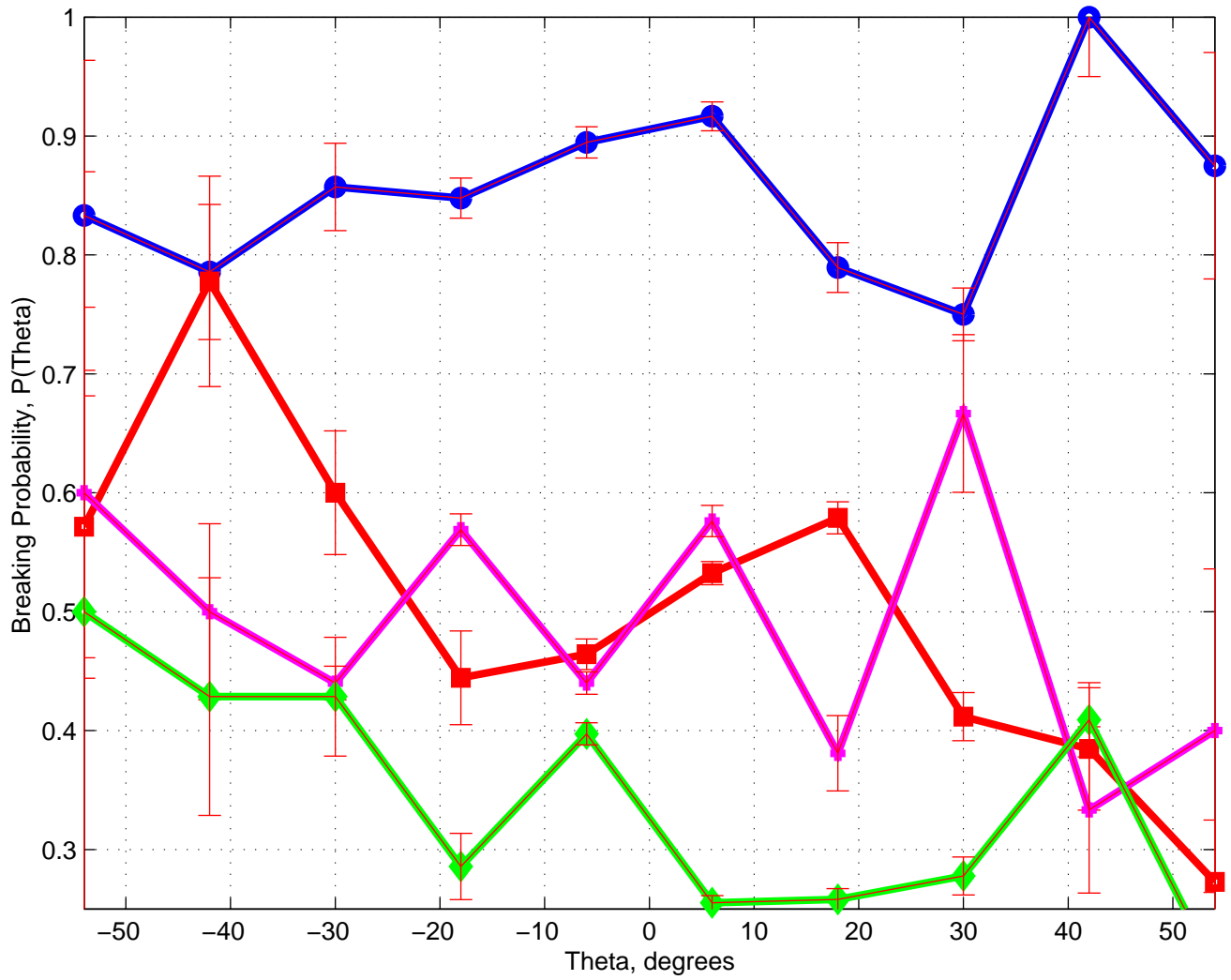


Figure 2.7: Breaking probabilities and 95% confidence interval for the four records.

III. COMPUTATION OF A NEW DISSIPATION TERM

A. Directionality and dissipation source term

1. The new dissipation source term

Based on the previous observations we have developed a new form of the saturation $B(k)$ in the dissipation source S_{ds} , which is now dependent on the direction. The S_{ds} form used here is a source term using a saturation threshold formulation (e.g. Banner et al, 2000, Alves et Banner, 2002, van derWesthuysen et al, 2007),

$$S_{ds}(\sigma, \theta) = -C_{ds} \left(\frac{B(\sigma, \theta)}{B_r} \right)^2 \sigma(k) E(\sigma, \theta) \quad (3.1)$$

Where $C_{ds} = 5.0 \cdot 10^{-5}$ and $B_r = 1.7 \cdot 10^{-5}$.

The form of the direction dependant saturation is given by:

$$B(\sigma, \theta) = \int_{\theta-\Delta\theta}^{\theta+\Delta\theta} C_g k^3 E(\sigma, \theta) d\theta = C_g k^3 \int_{\theta-\Delta\theta}^{\theta+\Delta\theta} E(\sigma, \theta) d\theta \quad (3.2)$$

The new source term has been implemented in the WAVEWATCH III code developed by Tolman et al. (1991). WAVEWATCH III predicts the spatial and temporal evolution of the wave spectra.

The underlying idea below this formulation is that the crests of waves propagating in quite the same direction ($\theta \pm \Delta\theta$) will travel a long time together and thus are more likely to break. Besides, the slope of a superpositions of two waves propagating in the same direction (with the same amplitude and wavenumber) is twice the initial slope whereas the slope of the same wave propagating orthogonally is only multiply by $\sqrt{2}$. The superposition of waves travelling in the same direction is thus more likely to induce white capping, consequently, the inherent severity may be higher. Therefore the spectral density around the direction considered may be important and that the reason for the integration around each direction θ . This leads us to redefine the threshold B_r which is then weighted to take into account the directional integration.

$$B_{rnew} = B_r \frac{\int_{-\pi}^{\pi} D(\sigma, \theta) d\theta}{\int_{-\Delta\theta}^{\Delta\theta} D(\sigma, \theta) d\theta}. \quad (3.3)$$

Where $D(\sigma, \theta)$ is the directional spreading function defined by $E(\sigma, \theta) = E(\sigma)D(\sigma, \theta)$ (Longuet-Higgins et al, 1963) and

$$D(\sigma, \theta) \propto \frac{1}{\cosh^2[2.5\theta]}, \quad (3.4)$$

This hypothesis is also broadly consistent with the observed change in threshold B_r with directional spread (Banner et al 2002).

2. Bimodal properties observations

Hwang et al 1999, investigate the directional spectral distribution by the mean of airborne measurements. Especially, the bimodal feature of the spectrum has generated much interest (eg, Banner and Young 1994, Young et al 1995). Numerical experiments proposed that this bimodal behaviour is controlled by the non-linear interactions (Komen et al. 1984, Young and Van Veddler 1993 and Banner and Young (1994)). Banner and Young (1994) suggest that the bimodal shape is due to the different

width of the wind input term S_{in} and of the dissipation term. S_{in} is narrower than S_{ds} , therefore the components oblique to the wind have a net energy loss between S_{in} and S_{ds} . Since the three major source terms S_{in} , S_{ds} , S_{nl} are coupled, the most important energy loss in the oblique directions is filled in by the non-linear interactions. The spectral directional distribution observations were deduced from three dimensional spatial topography measurements, acquired by an airborne scanning lidar. The main advantage of the 3D spatial data is the very high directional resolution. The data were acquired near Duck, North Carolina on 24 september 1997, between 1200 and 1600 UTC. Wind speed $U_{10}=9.5$ m/s and direction were quasi steady from 60 to 1300 UTC, then, from 1300UTC to 1600UTC, the wind speed decreases down to 5.5 m/s. The dominant measured wave number is $k_p = 0.098$ rad/m and the cooresponding dimensionless wave age U_{10}/c_p is thus about 1, where c_p is the peak phase velocity. To remain coherent with the observations, the results presented further correspond to the same wave age U_{10}/c_p .

3. Results

Our purpose here is to investigate whether or not such a change in the parametrization is supported by the observations. The numerical results obtain using the new source term are compared with Hwang et al's (1999) observations. We will particularly focus our attention on the bimodal properties. Although it is not the only relevant parameter to consider, the study remains judicious because wave models are still quite unable to represent these features. The computations were performed with both the Direct Interactions Approximation (DIA) and Webb-Resio-Tracy method (WRT). The second one provides an accurate estimation of the nonlinear interactions leading, in particular, to the bimodal spectral behaviour due to resonant interactions among spectral components. Furthermore two wind input source terms (differing by the width of their generated spectrum) were used in this study. This hypothesis is also broadly consistent with the observed change in threshold B_r with directional spread (Banner et al 2002). The wind speed is $U_{10} = 10$ m/s and the fetch unlimited. The results are presented under the shape of directional spectra at a waves age $a = c_p/U_{10} \sim 1$. This age was chosen so as to compare our results to observations (Hwang et al 2000). Several integration bandwidths $\Delta\theta$ are investigated and the related spectra are compared with spectra resulting from the full-bandwidth integrated saturation. The following table sums up the differents runs presented in the differents figures.

Figure	3.1	3.2	3.3	3.4
S_{nl}	DIA vs WRT	WRT	WRT	WRT
S_{in}	\cos^2	\cos vs \cos^2	\cos	\cos
S_{ds}	180° vs 60°	180° vs 60°	180° vs 80° , 80° , 60°	180° vs 80° , 80° , 60°

a. Effects of the interaction source term S_{nl} calculation

Due to its calculation cost the non-linear interaction source term S_{nl} is operationaly calculated by the Direct Interaction Approximation. Yet this approach cause damage on the directional distribution of S_{nl} . As said previously, not all the resonant configurations are considered Especially, the interactions which cause the spectral lobes are not represented. Web, Resio and Tracy proposed a calculation of the exact non-linear interaction referred to as WRT. The next figure present observed spectra and spectra calculated with the DIA and WRT code. For each case (WRT or DIA) the saturation $B(k, \theta)$ is calculated with different $\Delta\theta$. The results show a bimodal behaviour for spectra calculated with the WRT code, whereas, only one peak is observed for spectra obtain with the DIA. However, it is striking that the WRT spectra are narrower than DAI and observed spectra. Actually, the DIA is adjusted so as to fit the directional spread observations. It is likely that the parametrization of S_{in} and S_{nl} causes mistakes that cancelled together. In the next part another source wind input source term S_{in} is proposed so as to correct the width of the spectra. All the further calculations are computed with the WRT method.

b. Effects of the wind input source term shape

Based on Miles (1957) work, Janssen(1994) implemented a S_{in} of the form:

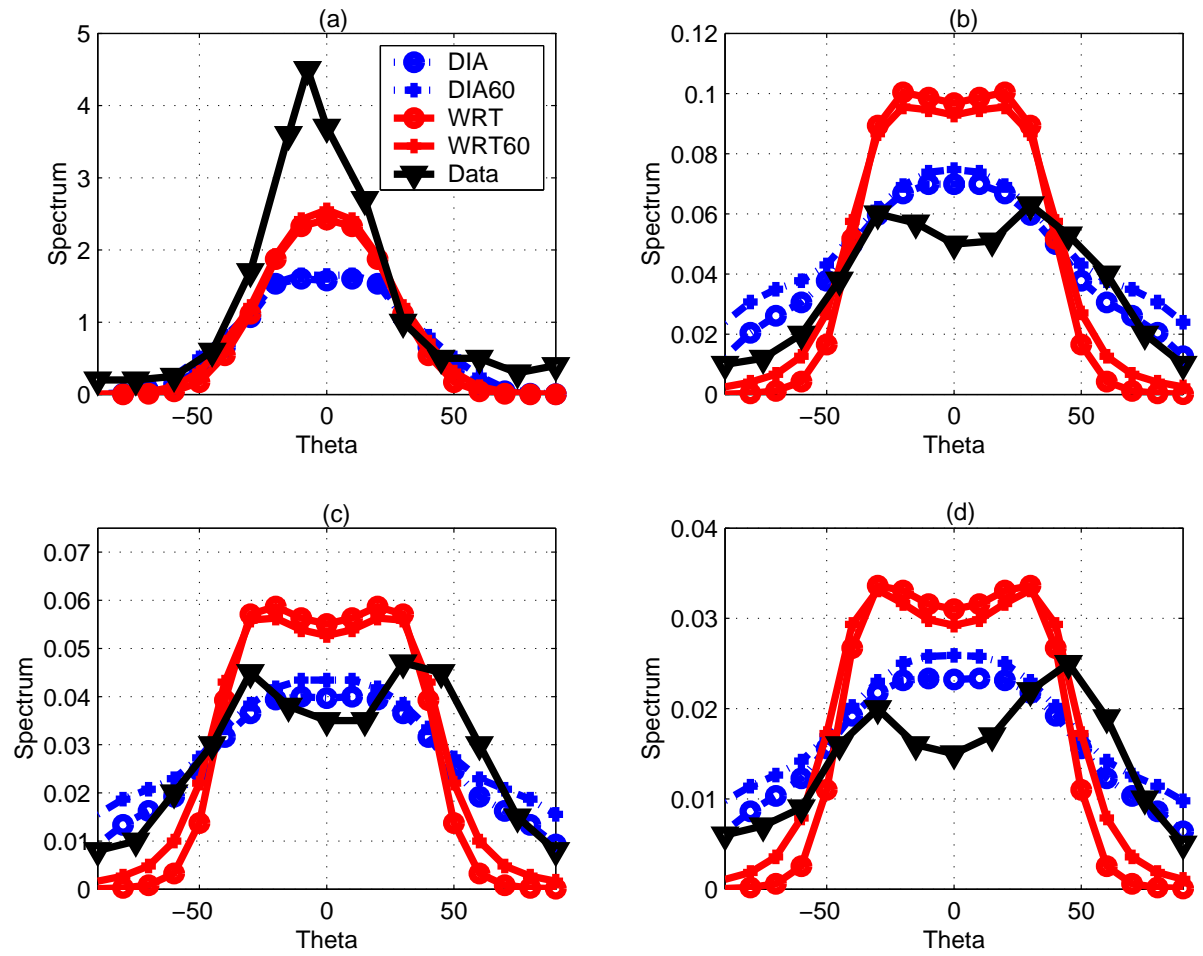


Figure 3.1: Wave spectra computed with the DIA and the WRT methods, with a full integrated saturation (referred to as DIA and WRT) and a saturation integrated over 60° (referred to as DIA60 and WRT60). All the computations are compared with observations. The different figures present the results and observations at different wavenumbers, (a): $k/k_p = 1$, (b): $k/k_p = 3.33$, (c): $k/k_p = 3.83$, (d): $k/k_p = 4.60$, with $k_p = 0.098$ rad/m.

$$S_{in} \propto \cos^2\theta \quad (3.5)$$

Where θ is the angle between the wind and wave propagation direction. Further we try another form of S_{in} which only differs by the exponent of the cosinus:

$$S_{in} \propto \cos\theta \quad (3.6)$$

As shown by figure 3.2, the spectral shape remain almost unchanged. The S_{in} term using a simple cosinus seems to provide spectra that are very slightly wider. Although the difference is minor, we will pursue our investigations using the S_{in} given by 3.6.

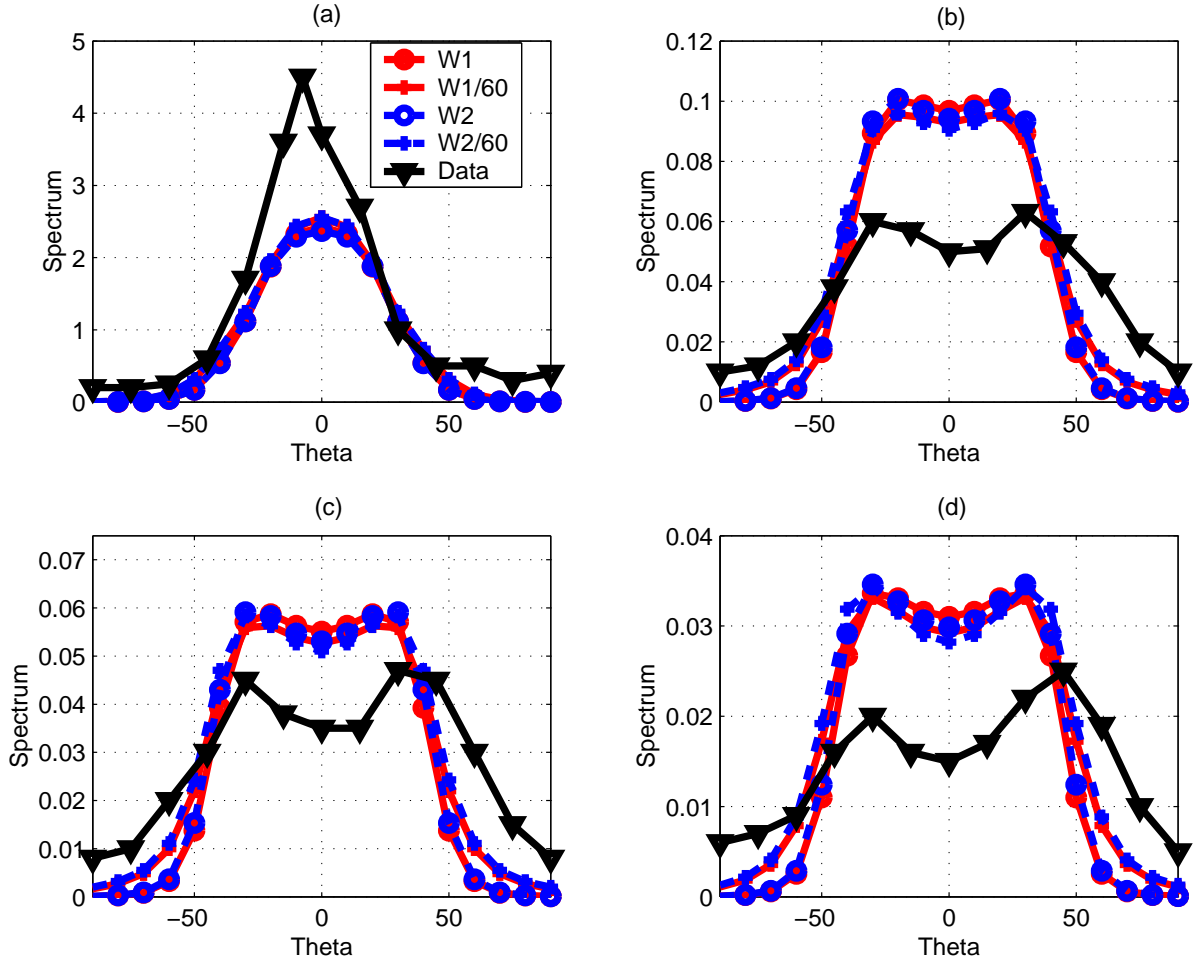


Figure 3.2: Wave spectra computed with the $S_{in} \cos$ form (W1) and the $S_{in} \cos^2$ form (W2), with a full integrated saturation (W1 and W2) and a saturation integrated over 60° of each side (W160 and W260). All the computations are compared with observations. The different figures present the results and observations at different wavenumbers, (a): $k/k_p = 1$, (b): $k/k_p = 3.33$, (c): $k/k_p = 3.83$, (d): $k/k_p = 4.60$, with $k_p = 0.098$ rad/m.

c. Directional integration and bimodal feature

In the present section, the saturation is integrated over several direction bandwidth $\Delta\theta$ and the resulting spectra are compared with the observations. The classical S_{ds} term is thus computed using $\Delta\theta = 180^\circ$, providing a full directional integration. So as to study in detail the bimodal spectral properties, let us introduce two new parameters r_{lobe} and θ_{lobe} . The lobe ratio r_{lobe} and angle θ_{lobe}

measure the lobes magnitude and angle. The figure 3.4 shows high great agreements between observed spectra and spectra computed with the 60° integrated saturation. The dissipation in a given direction seems then to be sensitive to the energy density of very far directions.

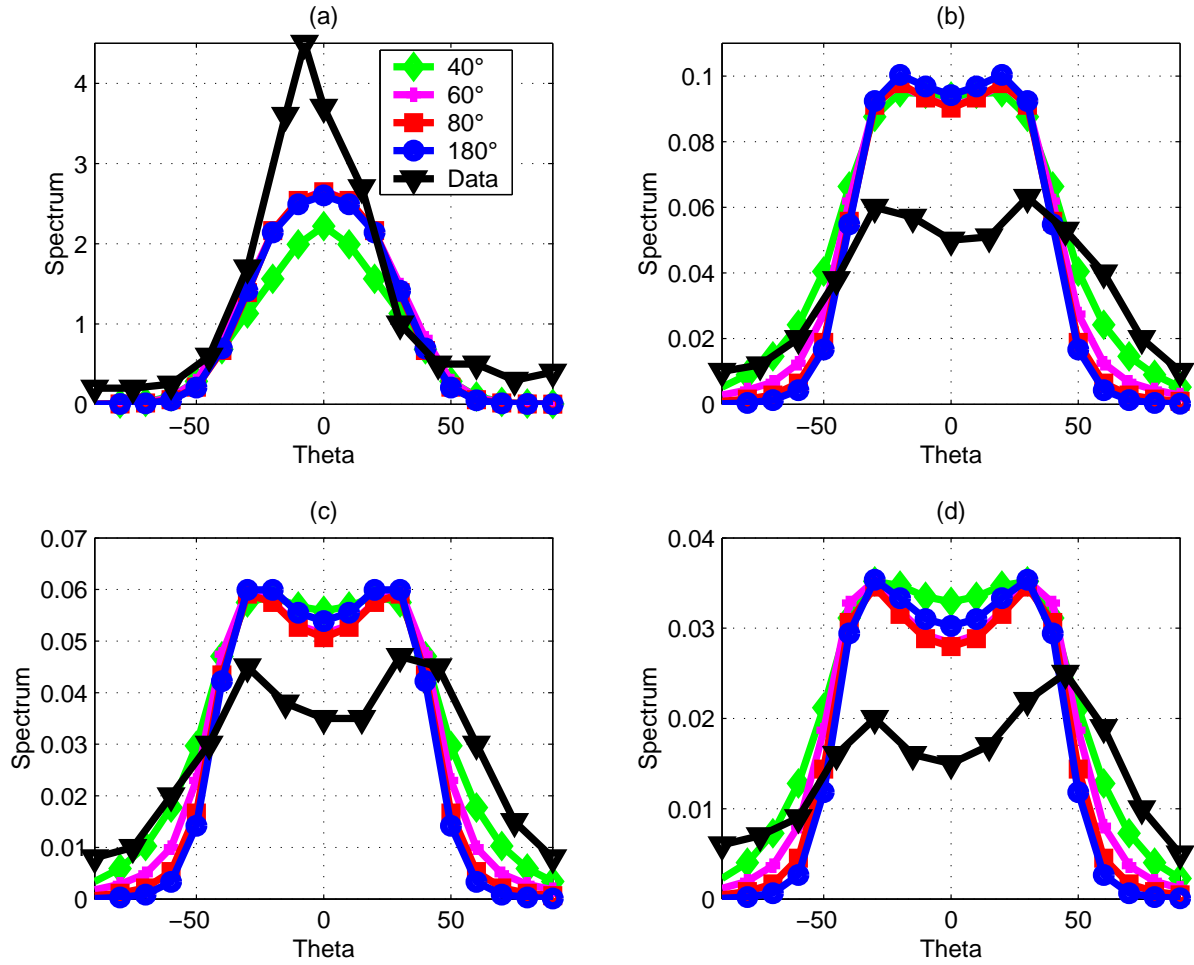


Figure 3.3: Wave spectra computed, with a full integrated saturation, referred to as 180° and saturations integrated over different width of each side referred to as 80° , 60° , 40° . All the computations are compared with observations. The different figures present the results and observations at different wavenumbers, (a): $k/k_p = 1$, (b): $k/k_p = 3.33$, (c): $k/k_p = 3.83$, (d): $k/k_p = 4.60$, with $k_p = 0.098$ rad/m .

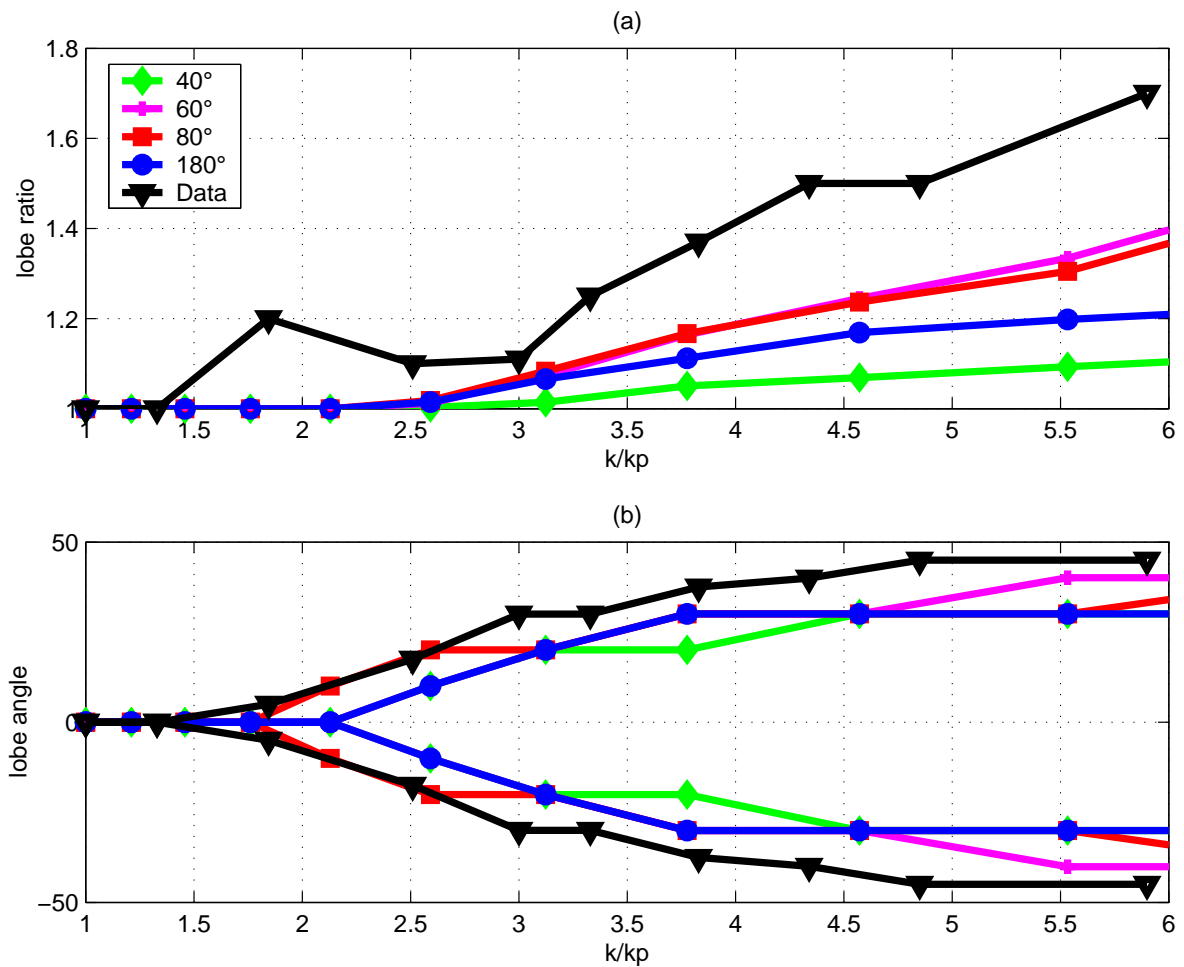


Figure 3.4: The upper panel shows the lobe magnitude r_{lobe} of spectra calculated with the direction dependant saturation, integrated over 180°, 80, 60°, 40°. The results are compared with observations. The lower panel shows the lobe angle θ_{lobe} of spectra calculated with the direction dependant saturation, integrated over 180°, 80, 60°, 40°. The results are compared with observations.

IV. CONCLUSION

Bimodal properties seem to be slightly better represented by the model using the the direction dependent dissipation. Especially, integration of the saturation over 60° wide provides better agreement with the observed r_{lobe} and θ_{lobe} observations. Thus, in that particular case, spectra computed with the new S_{ds} form are more realistic than those computed with the classical full integrated saturation. Yet, a lot of other spectral properties, such as the wave growth, the period prediction for example, still need to be validated. Moreover oblique fetch conditions, which are not well predicted by numerical models, could be tested to investigate whether or not the new dissipation term could bring improvements. The waves breaking observations did not provide evidence for a directional dependence of the breaking probability and severity. However, to conclude on that issue, many other waves observations, are obviously needed. Besides, longer times series containing therefore a larger number of waves, could also be usefull to obtains more reliable breaking statistics. Lastly, the analysis process is likely to induce mistakes in the interpretation of the observations. Among many other causes and although it is the most appropriate method, the WDM could cause misinterpretations, especially because it detects only one direction for each wave scale. Because wave dissipation is still not well undertood and since it impacts a large array of applications, investigations in that field deserve to be pursue.

Bibliography

- Alves, J. H. G. M. and M. L. Banner, 2003: Performance of a saturation-based dissipation-rate source term in modeling the fetch-limited evolution of wind waves. *J. Phys. Oceanogr.*, *33*, 1274–1298.
- Ardhuin, F., T. H. C. Herbers, G. P. van Vledder, K. P. Watts, 2007: A hybrid Swell and slanting-fetch on wind wave growth. *J. Phys. Oceanogr.*, *37*, 908–931.
- Ardhuin, F., 2007: Vagues: hydrodynamique et télédétection, Cours de seconde année, Master Mécanique-Physique.
- Banner, M. L., A. V. Babanin, I. A. Young, 2000: Breaking probability for dominant waves on the sea surface. *J. Phys. Oceanogr.*, *30*, 3145–3160.
- Banner, M. L., J. R. Gemmrich, D. M. Farmer, 2002: Multiscale Measurements of ocean wave breaking probability. *J. Phys. Oceanogr.*, *32*, 3364–3375.
- Babanin, A. V., I. R. Young, M. L. Banner, 2001: Breaking probabilities for dominant surface waves on water of finite depth. *J. Geophys. Res.*, *106*, 11,659–11,676.
- , Michael L. Banner and Russel P. Morison, 2006: On Modeling Spectral Dissipation due to Wave Breaking for Ocean Wind Waves. Proceedings of the 9th International workshop on wave hindcasting and forecasting, Victoria, Canada
- Babanin, A. V., I. R. Young, M. L. Banner, 2001: Breaking probabilities for dominant surface waves on water of finite depth. *J. Geophys. Res.*, *106*, .
- Babanin, A. V. and Y. P. Soloviev, 1998: Field Investigation of transformation of the wind wave frequency spectrum with fetch and the stage of development. *J. Phys. Oceanogr.*, *30*, 3145–3160.
- Bidlot, J., S. Abdalla, and P. Janssen, 2005: A revised formulation for ocean wave dissipation in CY25R1. Technical Report Memorandum R60.9/JB/0516, Research Department, ECMWF, Reading, U. K.
- Donelan, M. A., J. Hamilton, W. H. Hui, 1985: Directional spectra of wind-generated waves. *Phil. Trans R. Soc. Lond.*, *A315*, 509–562.
- Donelan, M. A. and W. M. Drennan, A. K. Magnusson, 1996: Nonstationary analysis of the directional properties of propagating waves. *J. Phys. Oceanogr.*, *26*, 1901–1914.
- Gemmrich, J. R. and D. M. Farmer, 2004: Near surface turbulence in presence of breaking waves. *J. Phys. Oceanogr.*, *34*, 1067–1086.
- Hwang, P. A. and D. W. Wang, 2000: Airborne measurements of the wavenumber spectra of ocean surface waves. Part II: Directional Distribution. *J. Phys. Oceanogr.*, *30*, 2768–2787.
- Janssen, P. A. E. M., 1991: Quasi-linear theory of wind-wave generation applied to wave forecasting. *J. Phys. Oceanogr.*, *21*, 1632–1642.
- Le Boyer, A., 2006: Dissipation de l'énergie des vagues. Mémoire de Master2 Physique, Océan, Atmosphère.
- Longuet-Higgins, M. S., 1973: A model of flow separation at a free surface. *J. Fluid Mech.*, *57*, 129–148.
- Long, C. E., D. T. Resio, 2007: Wind wave spectral observations in Currituck Sound, North Carolina. *J. Geophys. Res.*, *112*(C05001).
- Manasseh, R., A. V. Babanin, C. Forbes, K. Rickards, I. Bobevsky, A. Ooi, 2006: Passive acoustic determination of wave- breaking events and their severity across the spectrum. *J. Atmos. Oceanic Technol.*, *23*, 599–618.

- Melville, W. K., 1994: Energy dissipation by breaking waves. *J. Phys. Oceanogr.* , *24*, 2041–2049.
- Melville, W. K., P. Matusov, 2002: Distribution of breaking waves at the ocean surface. *Nature*, *417*, 58–63.
- Meyer, Y., S. Jaffard, O. Rioul, 1987: Analyse par ondelettes. *Pour la Science*, 28–38.
- Phillips, O. M., 1984: On the response of short ocean wave components at a fixed wavenumber to ocean current variations. *J. Phys. Oceanogr.* , *14*, 1425–1433.
- Phillips, O. M., 1985: Spectral and statistical properties of the equilibrium range in wind-generated gravity waves. *J. Fluid Mech.* , *156*, 505–531.
- Rasche N., F. Ardhuin, E. A. Terray, 2006: Drift and mixing under the ocean surface: a coherent one-dimensional description with application to unstratified conditions. *J. Geophys. Res.*, *111*(C03016).
- van der Westhuysen, A. J., M. Zijlema, Jurjen A Battjes, 2007: Nonlinear saturation based white-capping dissipation in SWAN for deep and shallow water *Coastal Engineering* , *54*, 151–170.
- Young, I. R., 1999: Wind generated ocean waves.. *Elsevier Science, Oxford* , 288 pp.
- Young, I. R., 2006: Spectral distribution of energy dissipation of wind-generated waves due to dominant wave breaking. *J. Phys. Oceanogr.* , *36*, 376–394.